Theoretically exact FBP reconstruction algorithms for two general classes of curves

Alexander Katsevich, Michael Kapralov

***Abstract*— We report on two extensions of exact FBP inversion formulas to more general classes of trajectories. The first class consists of curves C that are smooth, have positive curvature and torsion, and have some other natural geometric properties. We generalize the notion of PI-lines, study their properties and formulate a 1PI FBP reconstruction algorithm. The second class of trajectories constists of circle-plus curves, which have two components: C and L. The first component C, which is analogous to the circle in the traditional circle-plus trajectories, is essentially any closed (not necessarily planar) continuous curve. The second component L is almost any continuous curve. The only condition is that L starts below C and ends above C. The algorithm is especially convenient for the traditional circle-plus trajectories, which are implemented using a gantry and moving table. In this case we obtain a universal FBP algorithm, which is completely independent of how the table moves during the scan. The results of testing both algorithms demostrate good image quality.**

***Index Terms*— cone-beam, efficient inversion, exact inversion**

I. Introduction

A number of theoretically exact algorithms have been proposed in the past several years. They can be classified into three groups: filtered backprojection (FBP) algorithms, slow-FBP algorithms, and backprojection filtration (BPF) algorithms. Slow-FBP and BPF algorithms are quite flexible, allow some transverse data truncation, and can be used for virtually any complete source trajectory [12], [17], [13], [15], [16]. FBP algorithms are less flexible, but they are by far the fastest and have been developed for a range of source trajectories. They include constant pitch helix [6], dynamic pitch helix [9], [3], circle-and-line [5], circle-and-arc [7], [2], and saddle [14].

As the list presented above shows, until now FBP algorithms have been proposed only for certain types of well-defined trajectories: helices, saddles, etc. There was no FBP algorithm for a general class of curves. Ideally, such a class would be described only in terms of some basic geometric properties (e.g., smoothness, curvature, etc.) rather than specifying the types of curves (helices, etc.). In this paper we develop two theoretically exact shift-invariant FBP algorithms for two general classes of source trajectories. The first class consists of smooth curves C with positive curvature and torsion that also have some additional natural geometric properties that are discussed in section II-A. The inversion algorithm for these curves is a generalization of the formula proposed for constant- and variable-pitch helices in [6], [9]. The second result is an exact FBP algorithm for a class of generalized circle-plus trajectories. They consist of two components: C and L. The first component C, which is analogous to a circle in the traditional circle-plus trajectories, is essentially any closed (e.g., not necessarily planar) continuous curve. The second component L is almost any continuous curve, which starts below C and ends above C. Our class of curves encompasses practically all circle-plus trajectories that have been proposed in the literature so far and includes many more new ones, such as various saddle-plus trajectories, etc.

Department of Mathematics, University of Central Florida, Orlando, FL 32816-1364 *E-mail address:* akatsevi@pegasus.cc.ucf.edu, mikhail@mail.ucf.edu

II. Reconstruction for a general class of curves with positive curvature and torsion

The results presented in this section are based on [10].

A. PI lines and their properties

We start by defining PI lines for a general class of smooth curves and study their properties. Let C be a smooth curve:

$$I := [a,b] \ni s \to y(s) \in \mathbb{R}^3, \ |\dot{y}(s)| \neq 0. \tag{1}$$

Here and below the dot above a variable denotes differentiation with respect to s. Define the function

$$Q(s,s_0) := [y(s) - y(s_0), \dot{y}(s_0), \dot{y}(s)], \tag{2}$$

where $[e_1,e_2,e_3] := e_1 \cdot (e_2 \times e_3)$ is the triple product of vectors. If C is a helix, then Q is precisely the function that has been introduced under the same name in [9]. Similarly to [9], it turns out that Q is related to the uniqueness of PI-lines (see below). Given any $s_0, s_1 \in I$, $H(s_0,s_1)$ denotes the line segment with the endpoints $y(s_0), y(s_1) \in C$.

Definition 2.1: Pick two points $y(s_0), y(s_1) \in C$, $s_0 < s_1$. The line segment $H(s_0,s_1)$ is called a PI-segment if $Q(s,q) \neq 0$ for any $s,q \in [s_0,s_1]$, $s \neq q$.

Definition 2.2: Pick two points $y(s_0), y(s_1) \in C$, $s_0 < s_1$. The line segment $H(s_0,s_1)$ is called a maximal PI-segment if $Q(s_0,s_1) = 0$, but $Q(s,q) \neq 0$ for any $s,q \in (s_0,s_1)$, $s \neq q$.

If C is a helix, definition 2.1 gives the usual PI-segments $H(s,q), 0 < q-s < 2\pi$, and definition 2.2 gives the maximal PI-segments $H(s,s+2\pi)$.

In order to define our class of curves, we need to discuss how a smooth curve bends. Consider two points: $y(s_0), y(s) \in C$. Assume $y(s_0)$ is fixed, and $y(s)$ moves along C. The line segment joining $y(s_0)$ and $y(s)$ rotates about the instantaneous axis $e(s,s_0) = (y(s) - y(s_0)) \times \dot{y}(s)/|(y(s)-y(s_0)) \times \dot{y}(s)|$. The point $y(s)$ rotates also about the instantaneous axis which is obtained by finding the circle

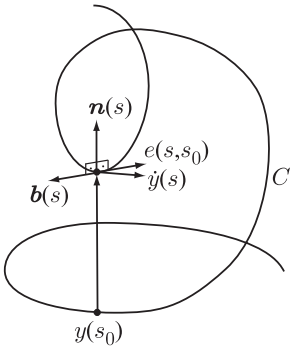

Fig. 1. Critical case

of curvature of C at $y(s)$ (also known as the osculating circle). The corresponding axis of rotation is $\mathbf{b}(s)$, i.e. the binormal vector. If $s \to s_0$, then $e(s, s_0) \to \mathbf{b}(s)$. Thus, the difference in directions of the two vectors can measure how much the curve bends between the two points. The maximum possible "bent" occurs when the two axes point in the opposite directions: $e(s, s_0) = -\mathbf{b}(s)$ (see Fig. 1).

We now formulate the main assumptions on the curve C:

C1. C is smooth, and the curvature and torsion of C are positive;

C2. C does not self-intersect within any PI-segment (or a maximal PI-segment) of C;

C3. Given any PI-segment (or a maximal PI-segment) $H(s_0, s)$ of C, there is no line tangent to C at $y(s_1)$ and intersecting C at $y(s_2)$ with $s_1, s_2 \in [s_0, s]$, $s_1 \neq s_2$;

C4. C does not bend too much, i.e. given any PI-segment (or a maximal PI-segment) $H(s_0, s)$ of C, one has $e(s_1, s_2) \neq -\mathbf{b}(s_2)$ for any $s_1, s_2 \in [s_0, s]$, $s_1 \neq s_2$.

If a curve satisfies conditions C1–C4, then its PI-segments have a number of nice properties. One of them is that no plane intersects $C(s_0, s_1)$ at more than three points.

B. Establishing uniqueness of PI lines

Fix $x \in U$. For each $s \in I$, fix a vector $N(s)$, $|N(s)| \equiv 1$ (a specific $N(s)$ will be chosen later). Define functions $q(s)$ and $\lambda(s)$ so that $H(s, q(s))$ is a PI-segment, $0 < \lambda(s) < 1$, and the point

$$x(s) := y(s) + \lambda(s)(y(q(s)) - y(s)) \in H(s, q(s)) \qquad (3)$$

has the property

$$x(s) - x \parallel N(s). \qquad (4)$$

We assume that the functions $q(s)$ and $\lambda(s)$ with the required properties exist. Later (see (7)) we find U such that for any $x \in U$ the functions $q(s)$ and $\lambda(s)$ do exist.

Condition (4) means that the parallel projection of $x(s)$ onto the plane through x with normal vector $N(s)$ coincides with x. Note that the vector-valued function $N(s)$ is determined independently of $q(s)$ and $\lambda(s)$. A similar idea is used in proving the uniqueness of PI lines for the standard helix (where the vector $N(s)$ is constant and directed along the axis of the helix). Denote $\Delta y(s) := y(q(s)) - y(s)$. Thus,

$$\varepsilon(s) := N(s) \cdot \{(y(s) + \lambda(s)\Delta y(s)) - x\} \qquad (5)$$

is the signed distance from $y(s)+\lambda(s)\Delta y(s)$ to x, i.e. $\varepsilon(s) = 0$ if and only if the chord $H(s, q(s))$ passes through x.

To find a set U where $\varepsilon'(s)$ is guaranteed to be positive for s in a chosen subinterval $I_0 \subseteq I$, we start by choosing a vector $N(s)$. Denote the supremum (respectively, infimum) of all q such that $H(s, q)$ is a PI line by $q_{max}(s)$ (respectively, $q_{min}(s)$). Define

$$N_\bullet(s) := \frac{y(q_\bullet(s)) - y(s)}{|y(q_\bullet(s)) - y(s)|}. \qquad (6)$$

Here and below $\bullet$ can be replaced with min or max. Thus, $N_\bullet(s)$ is the unit vector along $H(s, q_\bullet(s))$. We prove that $C(s, q_\bullet(s))$ lies on one side of the plane through $y(s)$ with normal $N_\bullet(s) \times \dot{y}(s)$, so it can be stereographically projected onto a plane not containing $y(s)$ with the same normal (this generalizes the projection onto the detector plane). It also turns out that the projected curves will be convex, as in the helical case. The parallel projection of $C(s, q_\bullet(s))$ onto $H^\perp(s, q_\bullet(s))$, which we denote by $\hat{C}(s, q_\bullet(s))$, is a closed convex curve that plays an important role in the definition of the set U where PI-lines are unique.

Even though the curve C is well-behaved locally, very little can be said about the global behavior of C. So we choose a "local" piece of C: $I_0 := [a_0, b_0] \subset (a, b)$. The word local is made precise later. For each $s \in I_0$ consider the curve $\hat{C}(s, q_{max})$ in the plane $N^\perp_{max}(s)$. Let $Cyl_{max}(s)$ be the infinite open cylinder with axis $N_{max}(s)$, whose base is the interior of $\hat{C}(s, q_{max})$. In the same fashion we define the cylinders $Cyl_{min}(s)$ using $\hat{C}(q_{min}, s)$ and $N_{min}(s)$. Define U as the intersection of all such open cylinders:

$$U := \cap_{s \in I_0} \left(Cyl_{min}(s) \cap Cyl_{max}(s)\right). \qquad (7)$$

If the curve turns too much, U can be empty. We assume that a sufficiently "local" piece of C is taken, so $U \neq \varnothing$. Note that in the case of helix all cylinders $Cyl_{min}(s)$ and $Cyl_{max}(s)$ are identical, so (7) gives the usual domain inside the helix. Uniqueness of PI lines for $x \in U$ is given by the following

Proposition 2.3: Pick $x \in U$. If x admits a PI-line, it is unique in the sense that there is no other PI-line with an endpoint inside I_0.

Combining all the results we obtain that the 1PI algorithm of [6] generalizes to curves that satisfy conditions C1–C4.

C. Numerical experiments

Numerical experiments have been conducted using flat detector geometry. The detector size is 1201×161, pixel size: $0.5 \times 0.5\text{mm}^2$ at isocenter, 1000 views are collected per rotation. The algorithm is implemented in native coordinates following [11]. We use the virtual detector, which always contains the x_3-axis. The clock phantom is chosen for reconstruction. The trajectory is a variable pitch/radius helix:

$$\begin{aligned} y(s) &= \left(R(s)\cos s, R(s)\sin s, \frac{h(s)}{2\pi}s\right), \\ h(s) &= h_0\left(1 + \frac{\sin(s/2)}{s}\right). \end{aligned} \qquad (8)$$

where $R = 600$mm and $h_0 = 35$mm. The projection of this trajectory onto the plane $x_3 = 0$ for $s \in [-2\pi, 2\pi]$ is shown in Fig. 2 (left panel). The boundary of the set

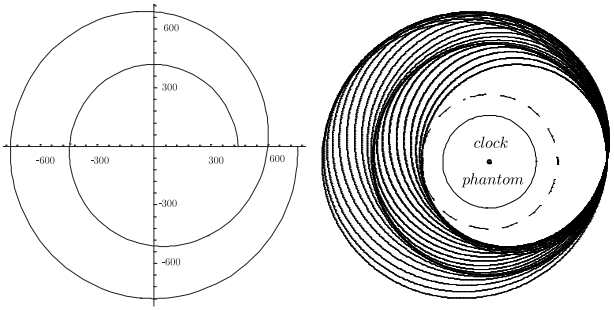

Fig. 2. Left panel: projection of the source trajectory in (8) onto the plane $x_3 = 0$. Right panel: the cross-section of the boundaries of $Cyl_{min}(s)$ and $Cyl_{max}(s)$ by the plane $x_3 = 0$.

U is calculated according to (7). The cross-section of the boundaries of cylinders $Cyl_{min}(s)$ and $Cyl_{max}(s)$ with the plane $x_3 = 0$ is shown in Fig. 2 (right panel). The solid circle of radius $r = 240$mm shows the boundary of the clock phantom, and the dashed circle is of the maximum radius $r \approx 348$mm that fits inside the cross-section of U. The result of reconstruction is shown in Fig. 3.

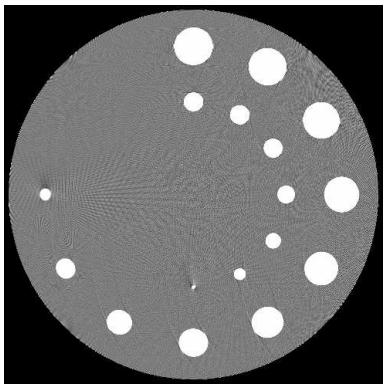

Fig. 3. Reconstruction of the clock phantom from trajectory (8): slice $x_3 = 0$, WL=0 HU, WW=100 HU.

III. Reconstruction for circle-plus trajectories

The results in this section are based on [8].

A. Algorithm

Let C be a piece-wise smooth closed curve, and L - an additional piece-wise smooth curve. Given $x \notin C \cup L$, let $\Xi_C(x)$ denote the set of planes through x which do not intersect C. Define U as the set of all x such that

L1. $\Xi_C(x) \neq \varnothing$, and

L2. for almost all $\Pi \in \Xi_C(x)$ the number of intersection points (IPs) in $\Pi \cap L$ is odd.

The main assumption about C and L is that U **contains an open set**. The first condition above is not restrictive. If $\Xi_C(x)$ is empty, then any plane through x intersects C, and L is not required for image reconstruction at x.

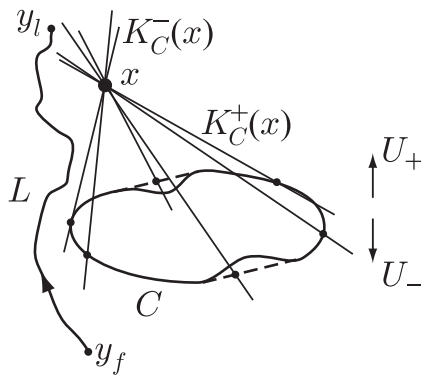

Fig. 4. Illustration of the cones $K_C^{\pm}(x)$

We now discuss the meaning of the second condition. For $x \in U$ define the cones (see Fig. 4):

$$\begin{aligned} K_C^+(x) := \{z \in \mathbb{R}^3 : z = \lambda_1(y_1 - x) + \lambda_2(y_2 - x), \\ y_1, y_2 \in C,\ \lambda_1, \lambda_2 > 0\}, \\ K_C^-(x) := \{z \in \mathbb{R}^3 : z = \lambda_1(y_1 - x) + \lambda_2(y_2 - x), \\ y_1, y_2 \in C,\ \lambda_1, \lambda_2 < 0\}. \end{aligned} \tag{9}$$

Let y_f and y_l be the first and last endpoints of L, respectively. The order of endpoints is determined according to the parametrization of L. Since U contains an open set, we can choose x not on the line through y_f and y_l. We show that only two cases are possible:

$$y_f \in K_C^+(x), y_l \in K_C^-(x) \text{ or } y_f \in K_C^-(x), y_l \in K_C^+(x). \tag{10}$$

Defining two sets

$$\begin{aligned} U_+ := \{x \in U :\ y_f \in K_C^+(x),\ y_l \in K_C^-(x)\}, \\ U_- := \{x \in U :\ y_f \in K_C^-(x),\ y_l \in K_C^+(x)\}, \end{aligned} \tag{11}$$

we show that $U = U_- \cup U_+$.

If the direction from y_f to y_l is called "upward", then we say that the points in U_- are below C, while the points in U_+ are above C (see Fig. 4). For the classical circle+line trajectory this definition gives the usual notions of "above the circle" and "below the circle". Summarizing, condition L2 above ensures that the endpoints of L be on opposite sides of C.

Following the general scheme proposed in [4], we define a normalized weight function. Let $n_c(\Pi)$ denote the number of IPs in $\Pi \cap C$, where Π is a plane through x.

1) If $n_c(\Pi) > 0$, each IP in $\Pi \cap C$ gets weight $1/n_c$, and each IP in $\Pi \cap L$ (if they exist) gets weight zero.
2) If $n_c(\Pi) = 0$, then the IPs in $\Pi \cap L$ get weights $+1, -1, +1, -1, \ldots, +1$, respectively.

Here we use the assumption that if Π does not intersect C, then the number of IPs in $\Pi \cap L$ is odd. The second rule above can be formulated as follows: odd-indexed IPs in $\Pi \cap L$ get weight +1, and even-indexed IPs in $\Pi \cap L$ get weight -1.

The main difference between the new algorithm and the one in [1] is the definition of the weight function in the case $n_c(\Pi) = 0$, i.e. when all the IPs are on L. In [1], the IP closest to C gets weight 1, while all other IPs get weight zero. It turns out that by assigning alternating weights +1 and -1 to the IPs

on L we get a much more flexible and simple algorithm, in which there is no need to filter along directions tangent to L.

The corresponding reconstruction algorithm is developed according to the general scheme in [4].

It turns out that the algorithm is essentially independent of the curve L. For each $y(s) \in L$ the only thing one needs to know is how C projects onto the detector. This projection depends only on the location of the detector and the coordinates of $y(s)$, but does not depend on the global properties of L. This property makes the algorithm especially convenient for circle-plus trajectories, which are implemented using a gantry and moving table. Regardless of how the table moves during the scan, in this case the curve L lies on the surface of the cylinder with base C. The projection of C onto the detector depends only on the axial distance between $y(s) \in L$ and the plane of the circle. Consequently, the algorithm is completely independent of the shape of L (as long as condition L2 is satisfied). This means, in particular, that the complete circle+line algorithm of [4] works for many other trajectories, e.g. circle+helix, circle+variable pitch helix, etc., without any modifications! Another implication is that in all these cases both the detector requirements and the axial extent of the additional scan L are exactly the same as in the circle+line case (cf. [4]).

B. Numerical experiments

To test our results, we conduct a numerical experiment with the clock phantom and circle+helix trajectory. The radius of the circle and the helix: 600mm, detector pixel size at isocenter: 0.910^{-3}rad $\times$ 0.5mm, detector size: 1024×325 pixels, number of views per turn (circle and helix): 1000.

The curve C is a circle of radius R in the plane $x_3 = 0$ and centered at the origin. The clock phantom is shifted by $\Delta x_3 = 40$mm up. This is done in order to better illustrate how the algorithm reconstructs cross-sections away from the plane of the circle. The curve L is a variable-pitch helix

$$y_1(s) = R\cos s,\ y_2(s) = R\sin s,\ y_3(s) = bs^2, \qquad (12)$$

where $b = 0.4$. We reconstruct the region where $y_3 > 0$, so only the portion of the helix corresponding to $s \geq 0$ is used.

For reconstructions we use the circle+line algorithm of [4]. As was already mentioned, the detector requirements and the axial extent of the helix are the same as in [4]. The only difference from [4] is that now we use the cylindrical detector geometry. According to the theory, the algorithm should work without any modifications and provide good image quality. It turned out to be the case. The results are shown in Fig. 5. As one sees, the image quality is consistent with a theoretically exact algorithm.

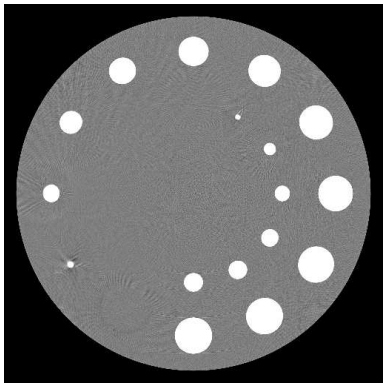

Fig. 5. Cross-section $x_3 = 40$mm through the reconstructed clock phantom. The region $|x_1|, |x_2| \leq 255.5$ is shown. WL=0HU, WW=100HU

ACKNOWLEDGMENT

The work of both authors was supported in part by NSF grant DMS-0505494.

REFERENCES

[1] C. Bontus, P. Koken, Th. Köhler, and R. Proksa. Circular CT in combination with a helical segment. *Physics in Medicine and Biology*, 51:107–120, 2007.

[2] G.-H. Chen, T.-L. Zhuang, S. Leng, and B. E. Nett. Shift-invariant and mathematically exact cone-beam FBP reconstruction using a factorized weighting function. *IEEE Transactions on Medical Imaging*, 2006. submitted.

[3] M. Kapralov and A. Katsevich. A 1PI algorithm for helical trajectories that violate the convexity condition. *Inverse Problems*, 22:2123–2143, 2006.

[4] A. Katsevich. A general scheme for constructing inversion algorithms for cone beam CT. *International Journal of Mathematics and Mathematical Sciences*, 21:1305–1321, 2003.

[5] A. Katsevich. Image reconstruction for the circle and line trajectory. *Physics in Medicine and Biology*, 49:5059–5072, 2004.

[6] A. Katsevich. An improved exact filtered backprojection algorithm for spiral computed tomography. *Advances in Applied Mathematics*, 32:681–697, 2004.

[7] A. Katsevich. Image reconstruction for the circle and arc trajectory. *Physics in Medicine and Biology*, 50:2249–2265, 2005.

[8] A. Katsevich. Image reconstruction for a general circle-plus trajectory. 2007. (submitted).

[9] A. Katsevich, Samit Basu, and Jiang Hsieh. Exact filtered backprojection reconstruction for dynamic pitch helical cone beam computed tomography. *Physics in Medicine and Biology*, 49:3089–3103, 2004.

[10] A. Katsevich and M. Kapralov. Efficient inversion of the cone beam transform for a general class of curves. 2006. (submitted).

[11] F. Noo, J. Pack, and D. Heuscher. Exact helical reconstruction using native cone-beam geometries. *Physics in Medicine and Biology*, 48:3787–3818, 2003.

[12] J. D. Pack, F. Noo, and R. Clackdoyle. Cone-beam reconstruction using the backprojection of locally filtered projections. *IEEE Transactions on Medical Imaging*, 24:1–16, 2005.

[13] E.Y. Sidky, Y. Zou, and X. Pan. Minimum data image reconstruction algorithms with shift-invariant filtering for helical, cone-beam CT. *Physics in Medicine and Biology*, 50:1643–1657, 2005.

[14] H. Yang, M. Li, K. Koizumi, and H. Kudo. Exact cone beam reconstruction for a saddle trajectory. *Physics in Medicine and Biology*, 51:1157–1172, 2006.

[15] Y. Ye, S. Zhao, H. Yu, and G. Wang. A general exact reconstruction for cone-beam CT via backprojection-filtration. *IEEE Transactions on Medical Imaging*, 24:1190–1198, 2005.

[16] T. Zhuang, S. Leng, B. E. Nett, and G. Chen. Fan-beam and cone-beam image reconstruction via filtering the backprojection image of differentiated projection data. *Physics in Medicine and Biology*, 49:1643–1657, 2004.

[17] Y. Zou, X. Pan, D. Xia, and G. Wang. PI-line-based image reconstruction in helical cone-beam computed tomography with a variable pitch. *Medical Physics*, 32:2639–2648, 2005.